Investigating the Impact from Ultrasonic Testing Uncertainty in Quantifying Ply Stack Orientation on the Probabilistic Failure Envelope

K. Rahul, D.A. Jack
Department of Mechanical Engineering, Baylor University

Abstract

Ultrasonic-Testing (UT) is one of the more popular techniques among Non-Destructive-Testing (NDT) for the inspection of manufactured and in-service components in automotive and aerospace industries. UT is used to identify defects, specifically delamination, damage, porosity, but not often used to correlate to that of the effective composite laminate properties. With the advancement of NDT waveform analysis to determine the ply-orientation of Carbon-Fiber-Reinforced-Polymers (CFRP) by recent researchers, the ability to determine the individual ply-orientation on a lamina-by-lamina basis has improved from an accuracy of ±10° to ±2° for each individual lamina. This paper investigates the impact of this improvement in resolution quantification on the confidence in characterizing the stiffness and strength of CFRP laminates from a UT data set. This is done by stochastically generating ply stack orientation from UT inspection results and quantifying the failure envelope from the Tsai-Wu failure model through a probabilistic Cumulative-Density-Function (CDF) of First Ply Failure (FPF) stresses using a Monte-Carlo Simulation technique. A variety of planar loads are generated to form the failure envelope for CFRP laminates consisting of 6, 12 and 16 plies for a variety of layup sequences (Unidirectional, Symmetric Cross Ply, Symmetric Quasi Isotropic, Multidirectional and Woven). As the ply stack quantification from UT data is stochastic, so is the confidence of the failure envelope. A comparative analysis of the stochastic failure envelope using the previous UT confidence (±10° for each individual lamina) and the recent UT analysis method confidence (±2° for each individual lamina) is provided to show the improvement in characterizing the probabilistic failure envelope. The recent high-resolution UT data analysis for ply orientation quantification is compared to earlier approaches for ply-orientation inspection, and results show a significant and measurable improvement in the confidence in the as-manufactured performance of the composite laminate.

Background

Currently, the trend of transition of the industries from metal to carbon fiber Laminates brings the opportunity for Non-Destructive Technique [1]. Current methods of interest are ultrasound inspection and X-ray CT inspection as most other NDT methos are not able to properly inspect the components, especially when the part is thick [2]. Currently, X-ray inspection methods are not popular due to their high cost of investment for both the equipment and the operators, nor is it readily deployable in the manufacturing environment. Ultrasonic testing (UT) is of interest in the present study due to its affordability, potential for portability to the manufacturing environment, and ease of training for a technician to inspect and analyze carbon fiber laminated parts.

Carbon fiber Laminates are being used in the industries due to their higher strength to weight ratio, better fatigue properties and corrosion resistance [3]. But the properties of the CFRP Laminates depend a lot on the manufacturing process, individual lamina orientation and numbers of plies used in the layup [4]. Of interest in the present paper is the sensitivity of the final part performance to changes in the individual ply orientations. Destructive testing, such as acid or burn testing, can be used to determine true ply orientations for each layer [2]. But a nondestructive test is preferred in many scenarios.

Smith and Clarke [5] investigated ply orientation from a UT Signal by visually scanning the C-scan image at various depths. Hsu et al. [6] were able to identify some misoriented ply orientation in laminates consisting of quasi-isotropic layup using cross-polarized shear waves based upon known signals of laminates properly manufactured. Komsky et al. [7] introduced the vector decomposition model which was later used by Hsu [8]. Hsu et al. [8] set a reduced vector decomposition model by orienting the transmitter to compute peak to peak amplitude to project and combine for a received signal that can detect misorientation in any certain ply. Park et al. [9] used 2D-FFT spatial spectrum to see the orientation of a misoriented ply in a 48-layer composite. Blackman and Jack [2] implemented the 2D FFT technique to predict each ply orientation with an average accuracy within 2 degrees for 98% of the lamina across a series of parts with thicknesses ranging from 3 to 18 lamina. They used a high-resolution ultrasonic c-scan technique with a 15 MHz transducer.

The present study uses several ply stacks from the work of Blackman and Jack [2] to use as seed information of the ply orientation. This present study investigates the sensitivity of the expected final part performance on the confidence of the ply stack, with the confidence values for the ply stack being based upon the work of [2]. The present work investigates four different ideal stacks with an assumed manufacturing variability, and then three stacks from the study provided in [2]. All computations are performed using a custom MATLAB code and the effective engineering properties and Tsai-Wu failure envelope is presented. As the study is for material specimen where the exact (deterministic) orientation is not known but instead there is uncertainty in the measured ply stack orientation, all results are presented using a probability density function (PDF) approach through the method of Monte-Carlo. In this work the probabilistic Cumulative-Density-Function (CDF) of First Ply Failure (FPF) stresses using Monte-Carlo Simulation technique are presented for each of the stacks investigated, and the results highlight the importance of including the stochastic nature of the ply configuration and not the assumed deterministic ply orientation.

Material and Manufacturing

For the analysis purpose of this paper several different stacking configurations are considered and are presented in Table 1.1 and 1.2. These include a series of more standard stacking configurations in Table 1.1 where both symmetry and balance are enforced along with a limitation to standard angles, 0^o, 30^o, 45^o, and 90^o. The non-standard configurations presented in Blackman and Jack given in Table 1.2 are selected to highlight the significant change in the failure nature of the composite as well as issues with sensitivity of the failure envelope to subtle variations in the ply stack due to the stochastic nature of fabrication and testing.

Table 1.1 Laminate stacking sequence.

Part Name	Number of Plies	Orientation
8C	8	[0/90/0/90/0/90/0/90]
12C	12	[0/90/0/90/0/90/0/90/0/90/0/90/]
16C	16	[0/90/0/90/0/90/0/90/0/90/0/90/0/90/0/90]
12M	12	[0/30/-30/45/-45/90/90/-45/45/-30/30/0]

Table 1.2 Laminate stacking sequence from Blackman and Jack [2]

Part Name	Number of Plies	Orientation after Burn Test
3B	3	[10/18/27]
6A	6	[70/60/19/42/29/46]
6C	6	[39/77/14/16/73/42]

MODELING OF CUMULATIVE DENSITY FUCNTION FOR FAILURE OF A COMPOSITE

The effective engineering properties are fully dependent on the individual composite lamina properties i.e., the modulus of elasticity in the longitudinal $\bar{E}_1$ and transverse $\bar{E}_2$ directions, Shear modulus in the plane $\bar{G}_{12}$ and Poisson's ratio in the plane $\bar{\nu}_{12}$ where the direction $\bar{x}_1$ is a local coordinate defined by the longitudinal axis of the fiber axis and $\bar{x}_2$ is transverse to the longitudinal axis of the fiber as depicted in Figure 2. For a unidirectional fiber, the $\bar{x}_2 - \bar{x}_3$ plane is a plane of symmetry, but for woven laminate the $\bar{x}_3$ axis is defined as the axis normal to the plane of the weave in the woven lamina. The failure criteria used in this study, Tsai-Wu [10], depends on the applied loads and material properties in both the tensile and longitudinal directions. The lamina longitudinal and transverse strengths are defined, respectively, as $\bar{F}_{1T}$ and $\bar{F}_{2T}$. The compressive longitudinal and transverse strengths are defined, respectively, as $\bar{F}_{1C}$ and $\bar{F}_{2C}$. The failure model used also requires the in-plane shear failure parameter defined as $\bar{F}_6$. For this study both unidirectional and woven CFRP laminate samples are investigated with the stiffness and failure properties used in the simulations for each material system listed in Table 2.1.

Table 2.1: Unidirectional and Woven Composite laminate properties

Laminate properties	Unidirectional Composite Properties [11]	Woven Composite Properties [12]
Longitudinal Modulus of elasticity, $\bar{E}_1$	135 GPa	36.1 GPa
Transverse Modulus of elasticity, $\bar{E}_2$	10 GPa	36.1 GPa
Poison's Ratio, $\bar{\nu}_{12}$	0.3	0.06
Shear Modulus, $\bar{G}_{12}$	5 GPa	3.65 GPa
Ultimate Longitudinal Compressive strength, $\bar{F}_{1C}$	1,200 MPa	355.8 MPa
Ultimate Longitudinal Tensile strength, $\bar{F}_{1T}$	1,500 MPa	407.6 MPa
Ultimate Transverse Compressive strength, $\bar{F}_{2C}$	250 MPa	355.8 MPa
Ultimate Transverse Tensile strength, $\bar{F}_{2T}$	50 MPa	407.6 MPa
Ultimate Shear strength, $\bar{F}_6$	70 MPa	100 MPa

Effective Stiffness

The effective Engineering Properties of the laminate i.e., the laminate's Youngs Modulus in the x_1 and x_2 directions are defined respectively as E_1 and E_2, are functions of the laminate thickness h and the extensional components of the compliance matrix $\boldsymbol{\alpha}$ as (see e.g., [4])

$$E_1 = \frac{1}{h\alpha_{11}} \tag{1}$$

$$E_2 = \frac{1}{h\alpha_{22}} \tag{2}$$

where the α_{11} and α_{22} are two of the components of the extensional compliance terms from the 3×3 $\boldsymbol{\alpha}$ matrix. In the present paper italic font is used for a scalar value and a bold font for matrices and tensors. The compliance matrix is found from the inverse of the stiffness matrix as

$$\begin{bmatrix} \boldsymbol{\alpha} & \boldsymbol{\beta} \\ \boldsymbol{\beta} & \boldsymbol{\delta} \end{bmatrix} = \begin{bmatrix} \boldsymbol{A} & \boldsymbol{B} \\ \boldsymbol{B} & \boldsymbol{D} \end{bmatrix}^{-1} \tag{3}$$

where $\boldsymbol{\beta}$ and $\boldsymbol{\delta}$ are not used in the present study. The $\mathbf{A}$, $\mathbf{B}$ and $\mathbf{D}$ terms in Equation (3) are found using classical laminate theory as (see e.g., [4])

$$\text{Extensional stiffnesses, } A_{ij} = \sum_{k=1}^{N_{lamina}} Q_{ij,k}\left(\bar{x}_{3,k} - \bar{x}_{3,k-1}\right) \tag{4}$$

$$\text{Coupling stiffnesses, } B_{ij} = \frac{1}{2}\sum_{k=1}^{N_{lamina}} Q_{ij,k}\left(\left(\bar{x}_{3,k}\right)^2 - \left(\bar{x}_{3,k-1}\right)^2\right) \tag{5}$$

$$\text{Bending stiffnesses, } D_{ij} = \frac{1}{3}\sum_{k=1}^{N_{lamina}} Q_{ij,k}\left(\left(\bar{x}_{3,k}\right)^3 - \left(\bar{x}_{3,k-1}\right)^3\right) \tag{6}$$

where $\{i,j\} \in \{1,2,3\}$. In the present study, $x_3 = 0$ corresponds to the through thickness midplane of the laminate, and the local coordinate system of the lamina, $\bar{x}_3$, aligns with the global coordinate axis x_3 for each of the individual lamina as depicted in Figure 2. In Equations (4)-(6) $\bar{x}_{3,k}$ is the position of the interfaces of the various lamina where the k is a counter. The $\bar{x}_{3,0}$ corresponds to the bottom face of the 1^{st} lamina, $\bar{x}_{3,N_{lamina}}$ corresponds to the bottom face of the last lamina, and $\bar{x}_{3,k}$ corresponds to the interface between the k and $k+1$ lamina for $k \neq \{0, n\}$ as shown in Figure 1. $\mathbf{Q}_k$ is the reduced stiffness matrix of the k^{th} lamina in the laminate coordinate frame (x_1, x_2, x_3). The reduced stiffness in the laminate frame $\mathbf{Q}_k$ is obtained from the reduced stiffness in the lamina frame $\bar{\mathbf{Q}}$ through the rotation tensor $\mathbf{T}_k$ as

$$\mathbf{Q}_k = (\mathbf{T}_k)^{-1}\bar{\mathbf{Q}}\,\mathbf{T}_\mathbf{k} \tag{7}$$

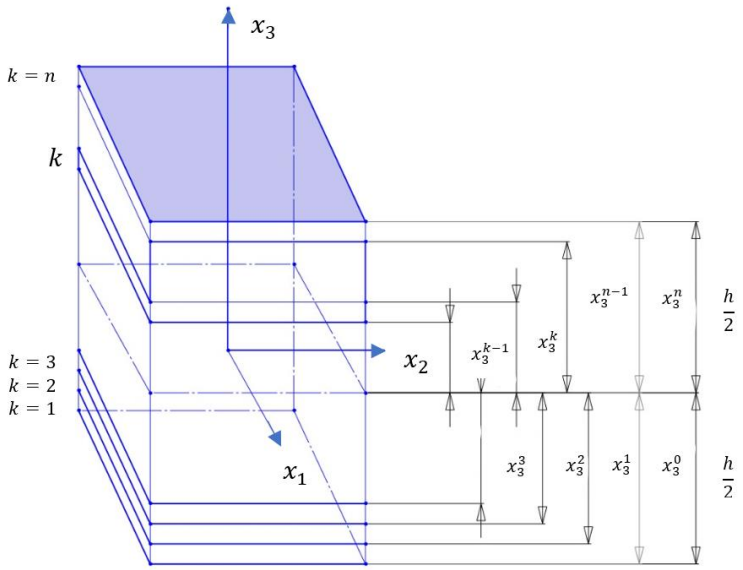

Figure 1 Composite ply stacking

The rotation tensor $\mathbf{T}_\mathbf{k}$ is used to rotate the reduced stiffness $\bar{\mathbf{Q}}$ from the lamina coordinate system $(\bar{x}_1, \bar{x}_2)$ to laminate coordinate system (x_1, x_2) as

$$\mathbf{T_k}(\phi_k) = \begin{bmatrix} \cos\phi_k{}^2 & \sin\phi_k{}^2 & 2\cos\phi_k \sin\phi_k \\ \sin\phi_k{}^2 & \cos\phi_k{}^2 & -2\cos\phi_k \sin\phi_k \\ -\cos\phi_k \sin\phi_k & \cos\phi_k \sin\phi_k & \cos\phi_k{}^2 - \sin\phi_k{}^2 \end{bmatrix} \tag{8}$$

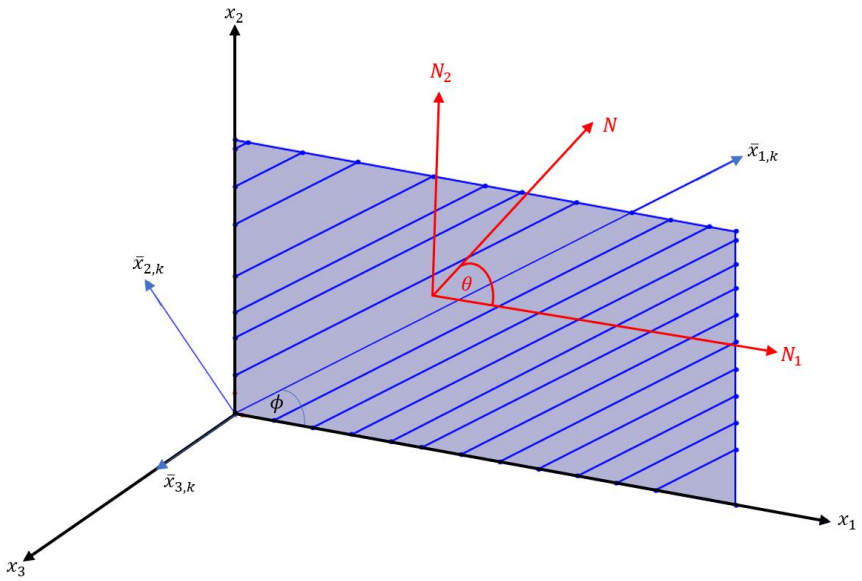

Figure 2 Composite ply stacking

Where, ϕ_k is the rotation angle between the principal axis of the lamina and the global x_1 coordinate as shown in Figure 2 of the k^{th} lamina. In the present study all lamina within a laminate are constrained to be fabricated from the same material, thus the reduced stiffness matrix $\bar{\mathbf{Q}}$ from Equation (7) is the same for all lamina and is defined as

$$\bar{\mathbf{Q}} = \begin{bmatrix} \bar{Q}_{11} & \bar{Q}_{12} & 0 \\ \bar{Q}_{21} & \bar{Q}_{22} & 0 \\ 0 & 0 & \bar{Q}_{66} \end{bmatrix} \tag{9}$$

The components of the reduced stiffness matrix $\bar{\mathbf{Q}}$ are obtained from the composite properties given in Table-2.1 as (see e.g., [4])

$$\bar{\nu}_{21} = \left(\frac{\bar{E}_2}{\bar{E}_1}\right)\bar{\nu}_{12} \tag{10}$$

$$\bar{Q}_{11} = \frac{\bar{E}_1}{(1 - \bar{\nu}_{12}\bar{\nu}_{21})} \tag{11}$$

$$\bar{Q}_{22} = \frac{\bar{E}_2}{(1 - \bar{\nu}_{12}\bar{\nu}_{21})} \tag{12}$$

$$\bar{Q}_{12} = \frac{\bar{\nu}_{21}\bar{E}_1}{(1 - \bar{\nu}_{12}\bar{\nu}_{21})} \tag{13}$$

$$\bar{Q}_{21} = \frac{\bar{\nu}_{12}\bar{E}_2}{(1 - \bar{\nu}_{12}\bar{\nu}_{21})} \tag{14}$$

$$\bar{Q}_{66} = \bar{G}_{12} \tag{15}$$

Tsai-Wu Failure Criteria

The general form of the Tsai-Wu [10] failure model is stated as

$$g(\mathbf{f},\mathbf{F},\boldsymbol{\sigma}) = \sum_{i=1}^{6} f_i\sigma_i + \sum_{j=1}^{6}\sum_{i=1}^{6} F_{ij}\sigma_i\sigma_j = 1 \tag{16}$$

where the stress tensor $\boldsymbol{\sigma}$ is written as a 6×1 array, $\sigma_i = \{\sigma_{11}, \sigma_{22}, \sigma_{33}, \sigma_{23}, \sigma_{13}, \sigma_{12}\}$, and $\{i,j\} \in \{1,2,\dots,6\}$. In the present study plane stress is assumed for the loading which implies $\sigma_{33} = \sigma_{23} = \sigma_{13} = 0$. When $g(\mathbf{f},\mathbf{F},\boldsymbol{\sigma}) > 1$ failure will occur and when $g(\mathbf{f},\mathbf{F},\boldsymbol{\sigma}) < 1$ the composite has not yet failed [10]. Accounting for plane stress, the Tsai-Wu failure model simplifies to

$$f_1\sigma_1 + f_2\sigma_2 + F_{11}\sigma_1\sigma_1 + F_{22}\sigma_2\sigma_2 + F_{66}\sigma_6\sigma_6 + 2F_{12}\,\sigma_1\sigma_2 = 1 \tag{17}$$

where the failure coefficients f_i and F_{ij} are given as (see e.g., [13])

$$f_1 = \frac{1}{\bar{F}_{1T}} - \frac{1}{\bar{F}_{1C}} \tag{18}$$

$$F_{11} = \frac{1}{\bar{F}_{1T}\bar{F}_{1C}} \tag{19}$$

$$f_2 = \frac{1}{\bar{F}_{2T}} - \frac{1}{\bar{F}_{2C}} \tag{20}$$

$$F_{22} = \frac{1}{\bar{F}_{2T}\bar{F}_{2C}} \tag{21}$$

$$F_{66} = \frac{1}{\bar{F}_6^2} \tag{22}$$

$$F_{12} = -\frac{1}{2\sqrt{F_{11}\,F_{22}}} \tag{23}$$

The stress of the k^{th} lamina in the laminate coordinate system is given in terms of the lamina coordinate system as

$$\begin{bmatrix}\sigma_{11}\\ \sigma_{22}\\ \sigma_{12}\end{bmatrix}_k = \boldsymbol{T_k}\begin{bmatrix}\bar{\sigma}_{11}\\ \bar{\sigma}_{22}\\ \bar{\sigma}_{12}\end{bmatrix}_k \tag{24}$$

and the stress relates to the strain in the k^{th} lamina through the stiffness matrix as

$$\begin{bmatrix}\sigma_{11}\\ \sigma_{22}\\ \sigma_{12}\end{bmatrix}_k = \boldsymbol{Q_k}\begin{bmatrix}\epsilon_{11}\\ \epsilon_{22}\\ 2\epsilon_{12}\end{bmatrix}_k \tag{25}$$

The strain in the individual lamina, ϵ_{ij} can be written in terms of the neutral axis (a.k.a. midplane) strain $\boldsymbol{\epsilon}^0 = \{\epsilon_{11}^0, \epsilon_{22}^0, 2\epsilon_{12}^0\}$ and the laminate curvature $\boldsymbol{\kappa} = \{\kappa_{11}, \kappa_{22}, \kappa_s\}$ as

$$\begin{bmatrix}\epsilon_{11}\\ \epsilon_{22}\\ 2\epsilon_{12}\end{bmatrix}_k = \begin{bmatrix}\epsilon_{11}^0\\ \epsilon_{22}^0\\ 2\epsilon_{12}^0\end{bmatrix}_k + x_{3,k}\begin{bmatrix}\kappa_{11}\\ \kappa_{22}\\ \kappa_s\end{bmatrix}_k \tag{26}$$

Applying a force $\mathbf{N} = \{N_1, N_2, N_3\}$ and moment $\mathbf{M} = \{M_1, M_2, M_3\}$, the midplane strains and the curvatures are found by

$$\begin{bmatrix} \boldsymbol{\epsilon}^0 \\ \boldsymbol{\kappa} \end{bmatrix} = \begin{bmatrix} \boldsymbol{\alpha} & \boldsymbol{\beta} \\ \boldsymbol{\beta} & \boldsymbol{\delta} \end{bmatrix} \begin{bmatrix} \boldsymbol{N} \\ \boldsymbol{M} \end{bmatrix} \tag{27}$$

Monte Carlo Simulation

Monte Carlo simulation is a very strong tool for statistical analysis. It uses random numbers to generate a mathematical model for further statistical analysis (see e.g., [14]). The purpose of this study is to determine the effective stochastic failure envelope for a given laminate. The reason for the stochastic failure envelope instead of a deterministic envelope is due to the angle uncertainty from the measurement of the ply orientation using the non-destructive high-resolution ultrasonic approach introduced by Blackman and Jack [2]. The process is composed of three broad steps, defining the material properties of the lamina, randomly generating N_{sample} samples of the individual lamina orientations from the characterized lamina orientation, and generating the failure envelope for the randomly sampled laminate orientation stack. For the first step we use the properties in Table 2.1. The samples are all assumed to follow a standard normal distribution as

$$P(\phi, \mu, \lambda) = \frac{1}{\lambda\sqrt{2\,\pi}} e^{-(\phi-\mu)^2/\lambda} \tag{28}$$

based upon the observations in [2]. In Equation (28) μ is the mean of the distribution and λ is the standard deviation about the mean. An individual lamina is then randomly sampled from the distribution in (28). This process is repeated for each individual lamina $k \in \{1,2, \dots, N_{lamina}\}$ where the mean value is defined by the characterized lamina orientation, such as given in Table 1.1 and 1.2, and the mean value for each lamina is based upon the confidence from the characterization method. This stochastic sampling generates a series of angles for each lamina from the n^{th} simulation as $\phi_{k,n}$. Once the orientation stack $\phi_{k,n}$ for the given simulation is defined, the A_{ij}, B_{ij} and D_{ij} matrices from Equations (4)-(6) can be evaluated using the rotation matrix in (7). These stiffness matrices are then saved for later analysis.

Next a load along the angle projection θ_m, shown in Figure 2, is identified for a given laminate sample. The load is defined as

$$\boldsymbol{N}_m = a\{cos\,\theta_m, sin\,\theta_m, 0\} = \{\sigma_1, \sigma_2, 0\} \tag{29}$$

The value of a is changed until the failure envelope boundary along the projection θ_m is identified. This occurs when the left-hand side of Equation (17) is equal to 1. This is done by evaluating Equation (*27*) for the given projection, for the given laminate stack, and then evaluating Equation (*24*) which in turn is used to evaluate Equation (17).

Results and Analysis

Effective Stiffness

The first study presented is for a 3-lamina sample in Table 1.2 labeled 3B, a [10/18/27] stack, which defines the mean of the distribution function μ_k. In all studies in this section, $N_{sample} = 1{,}000$ is used to generate 1,000 randomly sampled laminate layups. The standard deviation λ_k is set to either 2° or 10° for this and all subsequent studies in this paper. The value for 2° is selected based upon the high resolution inspection data found in [2], whereas the value for 10° is based upon the earlier studies by the group identified in[2]. The thickness of an individual lamina is set to 0.125 mm, thus the laminate thickness is $h =$

$N_{lamina} \times 0.125$ mm. Using Equations (3) to (15) and h, the effective Young's Modulus value E_1 for the laminate from Equation (1) are calculated for each of 1,000 samples. The histogram of the effective moduli for Sample 3B is shown in Figure 3 and Figure 4 for E_1. Considering the 3B sample from [2] it is seen that an error of 2°, shown in Figure 3, while measuring ply orientation can cause a variation of normalized E_1 values from 32 GPa to 50 GPa. Conversely, and error of 10°, shown in Figure 3, while measuring ply orientation can cause a variation of normalized E_1 values from 13 GPa to 125 GPa. Notice that the spread of the moduli value E_1 is greatly reduced with the higher resolution scan data as seen in Figure 3. A similar study can be presented for the transverse modulus E_2 using Equation (2) yielding similar conclusions. The effective stiffness of a composite depends on the composite properties and the individual ply orientations, thus a higher confidence in the ply orientation will results in a higher confidence in the expected values of the moduli.

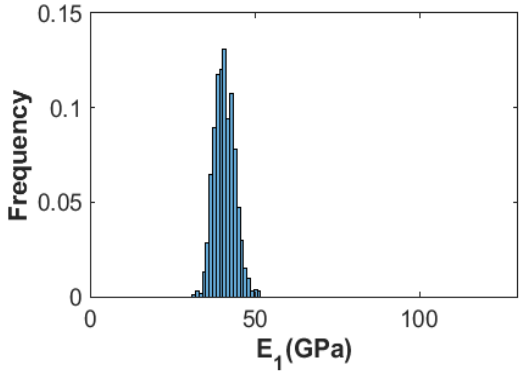

Figure 3 Variation of Effective Engineering Properties for 2° deviation, E_1 (Sample 3B)

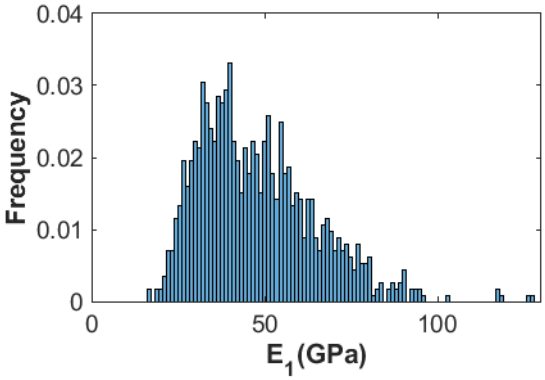

Figure 4 Variation of Effective Engineering Properties for 10° deviation, E_1 (Sample 3B)

Failure Envelope

To describe the failure envelope Sample 12C from Table 1.1 is taken which is a symmetric 12-lamina consisting of 0° and 90°. From the 1000 samples of randomly sampled laminate layups the 1st, 400th and 1000th simulations are picked at random to illustrate the variation in the failure envelope, and the results are shown in Figure 5. The failure envelope is generated with the angle θ_m for Equation (29) varying from 0° to 360° with an increment of 1°. Using the midplane strains found from Equation (27) strains in individual lamina are calculated by using Equation (26) which is used to find the stresses in each lamina through the reduced stiffness matrix, $\mathbf{Q}_k$ and rotation matrix, $\mathbf{T}_k$ from Equation (25) and (24). The First Ply Failure longitudinal σ_1 and transverse σ_2 stresses are calculated from the stresses found for an angle θ_m using Equation (17). For the case of Sample 12C, a 12-ply symmetric cross ply composite, the variation of failure envelope is quite significant as seen from the three Monte-Carlo simulations shown in Figure 5.

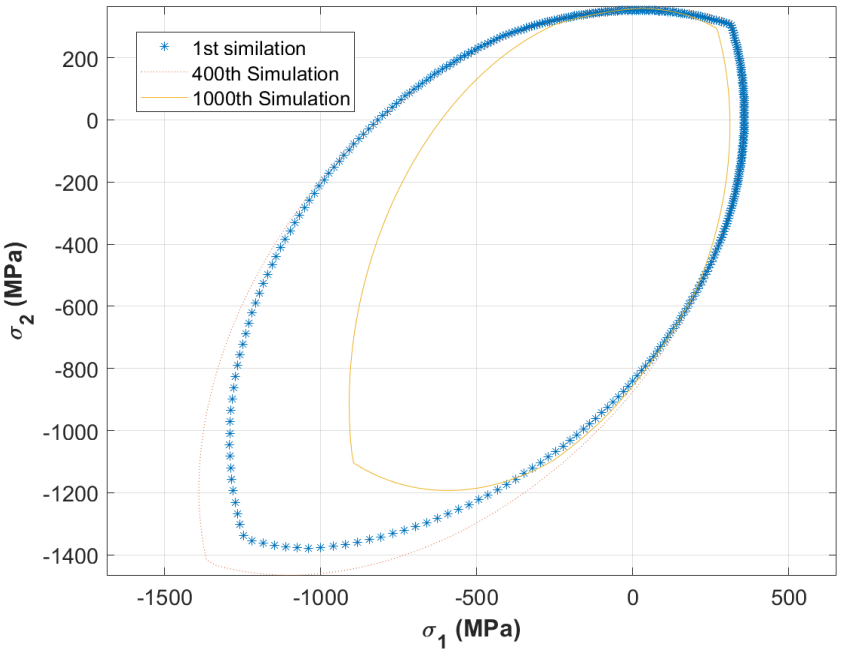

Figure 5 Failure Radius variation for 20 deviations (Sample 12C)

A comparative study of the error found between the recent non-destructive inspection method for ply detection as compared to the previous method for the Sample 12M ply-stacking sequence, a 12 multidirectional lamina composite panel. The Cumulative Density Function (CDF) plot is used to present the stochastic variation from the 1,000 various samples. The results of the CDF, shown in Figure 6, indicates the safe region for loading by the blue color and the loading states that would cause a failure in red. A value of 1 indicates no failure envelope includes the depicted loading state. For example, a load of $\mathbf{N} = \{-1{,}000MPa, -1{,}000MPa, 0\}$ has a CDF of 1 for both the 2° and 10° variation specimen implying this loading state would fail every single one of the laminate stacks. A load of $\mathbf{N} = \{-250MPa, -250MPa, 0\}$ has a CDF of 0 for both the 2° and 10° variation specimen and thus would have no failures. Conversely, a load of $\mathbf{N} = \{-1{,}100MPa, -950MPa, 0\}$ has a CDF of 0 for the data from 2° inspection stack whereas the CDF using the stack from the 10° inspection stack has a CDF of 0.48, corresponding to an estimate that 48% of the laminates would fail this loading configuration. Another way of stating this is that the results from an inspection with a confidence of 2° would lead the analyst to conclude that the loading condition of $\mathbf{N} = \{-1{,}100MPa, -950MPa, 0\}$ was safe, whereas an inspection having access to a system with a confidence of 10° would conclude the same loading condition was not safe with a near 50% likelihood of failure. Thus, having access to lower quality inspection data will lead one to either repair or scrap a functional and safe part unnecessarily.

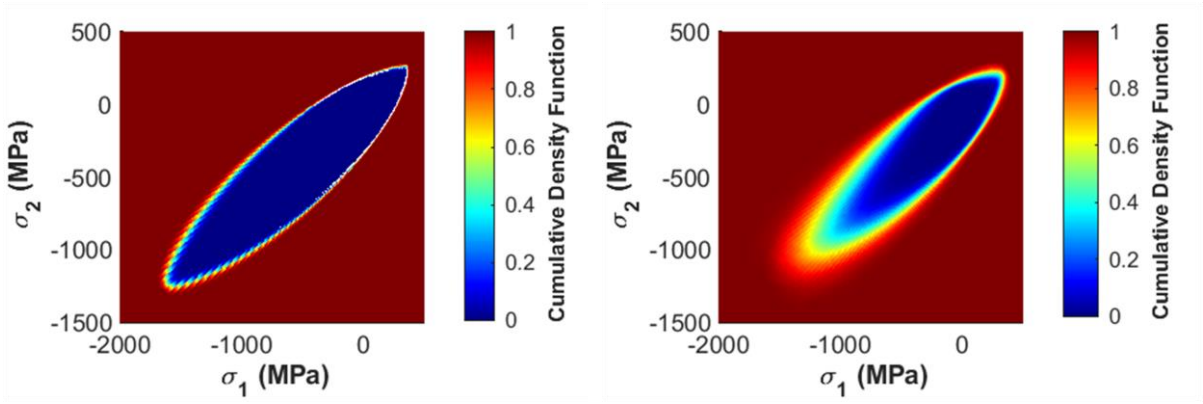

(a) (b)

Figure 6 CDF variation of failure envelope (Sample 12M) (a) 2° confidence in inspection, (b) 10° confidence in inspection

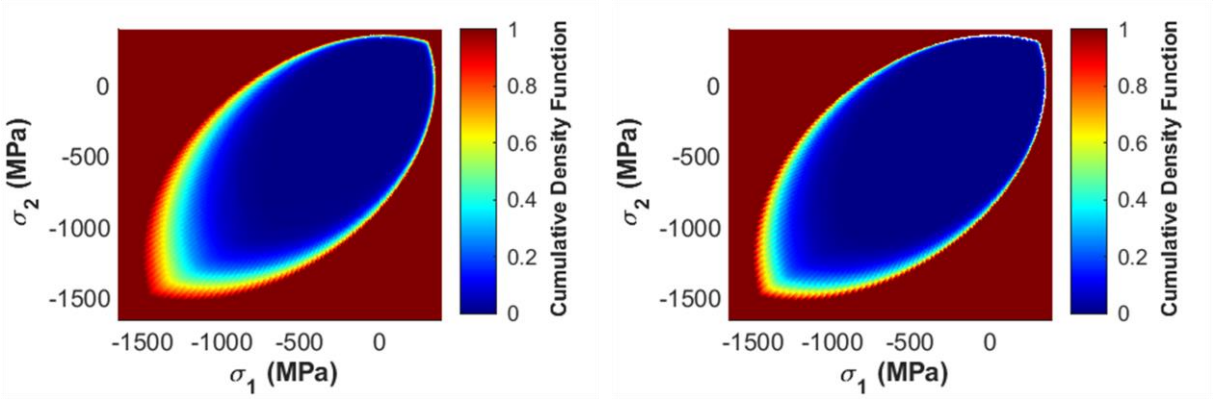

(a) (b)

Figure 7 Failure Envelope variation for different ply numbers, both with a 2° confidence in the ply stack orientation (a) Sample 8C, (b) Sample 16C

A different study is presented in Figure 7, for a composite inspected using a system that yields a 2° confidence. The stack in Figure 7(a) is an 8-layer cross-ply composite whereas the stack in Figure 7(b) is a 16-layer cross-ply composite. Notice that the transition of the CDF from a value of 0 (no failure) to 1 (all failure) becomes narrower with the increase in the number of lamina. The authors have performed a similar study of increasing the number of lamina in the stack for other ply stack configurations like Unidirectional, Symmetric Quasi Isotropic, Multidirectional and Woven composites consisting of 6, 12 and 16 layers, and the conclusion that the sensitivity to the ply variability decreases with increasing number of lamina in the stack is consistent across all studies.

One final study is for the non-symmetric, non-balanced untraditional ply stack configuration, specifically sample 6A from Table 1.2. This configuration was used in the FAA certification study of Blackman and Jack to test the viability of the inspection system. In this final study both the 2° and 10° deviation in the inspected orientation is assumed as above. Viewing **Error! Reference source not found.** the first feature to notice is that the shape of the failure envelope is different than that of the traditional ply stacks studied above. Regardless, the conclusion is the same as in the previous studies that the 2° confidence simulation

yields a narrower transition between the safe and failed regions versus that of the 10° confidence simulation. In addition, as before, the safe region of the failure envelope itself is smaller for that of the 10° simulation suggesting that a part would be more likely to be considered insufficient for a given loading state than is actually the true load carrying capacity of the laminate.

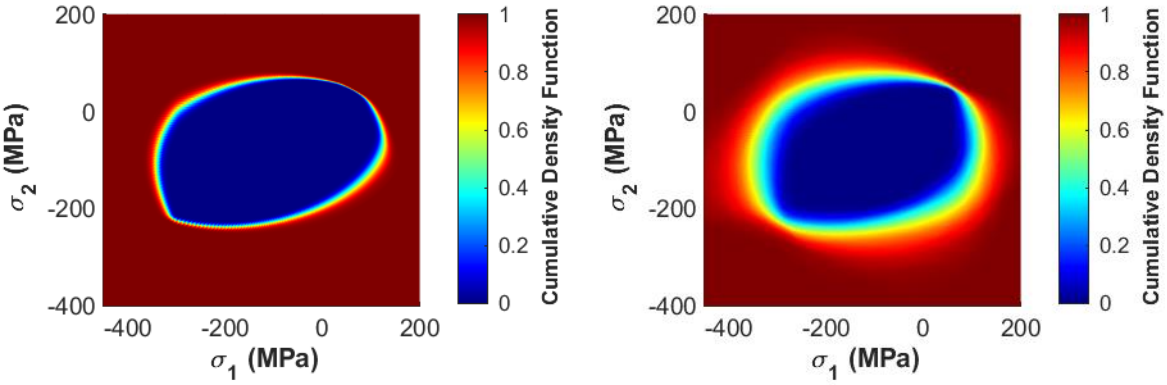

Figure 8 CDF variation of failure envelope (Sample 6A) (a) 2° confidence in inspection and (b) 10° confidence in inspection

Conclusion

This paper has presented a method to generate the cumulative density function failure envelope for a laminated composite. This method was used to analyze the impact of UT data accuracy to determine ply orientation on the engineering structural properties and failure envelope of CFRP laminates. An algorithm for determining the expected stiffness and failure criteria using the Tsai-Wu failure model is coupled in this work to a number of Monte-Carlo simulation to generate the expected composite properties from an error in quantification from a ultrasonic inspection data set. The work of this paper was able to provide a statistical analysis for several traditional laminate stacks along with a several from an earlier experimental study coupled with inspection. The algorithm provides a justification of the methods used to determine ply orientation from UT system data.

From the analysis, it can be inferred that, for some special types of orientation stacks, a reduced confidence in quantifying the ply orientation can cause a drastic change in the expected effective material properties and failure envelope of a composite. So, for industrial use safety factors needs to be implemented if poor quality UT data was utilized in any decision process, and for several samples in the present study poor quality UT data would suggest the need to fail or repair a part unnecessarily.

Bibliography

[1] R. Smith, L. Nelson, M. Mienczakowski, and R. Challis, “Automated analysis and advanced defect characterisation from ultrasonic scans of composites,” *Insight - Non-Destructive Testing and Condition Monitoring* · February 2009, doi: 10.1784/insi.2009.51.2.82.

[2] Nathaniel J. Blackman and D. Jack, “Novel Technique for the Automated Determination of the Ply Stack for a Woven Carbon Fiber Composite using High-Frequency Pulse Echo Ultrasound,” Sep. 08, 2021.

[3] A. Morabito, “What Industries Use Carbon Fiber?” *Element6 Composites*. https://element6composites.com/what-industries-use-carbon-fiber/

[4] Ever J Barbero, “Introduction to Composite Materials Design -- Third Edition.” https://barbero.cadec-online.com/icmd/
[5] R. A. Smith and B. Clarke, “Ultrasonic C-scan determination of ply stacking sequence in carbon-fibre composites,” *Insight - Non-Destructive Testing and Condition Monitoring,* Vol. 36, Issue. 10, Pages. 741–747, 1994.
[6] D. K. Hsu and B. A. Fischer, “Detection of layup errors in prepreg laminates using shear ultrasonic waves,” Nondestructive Evaluation Techniques for Aging Infrastructure and Manufacturing, Pages. 279–286. Nov. 1996, doi: 10.1117/12.259209.
[7] I. N. Komsky, I. M. Daniel, and Y.-C. Lee, “Ultrasonic determination of layer orientation in multilayer multidirectional composite laminates,” *Review of progress in quantitative nondestructive evaluation.* Vol. 11B, Pages. 1615–1622, Jan. 1992.
[8] “Characterization of CFRP Laminates’ layups using through-Transmitting ultrasound waves,” *KSME International Journal*, March. 2002.
[9] J. W. Park, K. H. Im, D. K. Hsu, S. W. Na, Y. N. Kim, and I. Y. Yang, “Ultrasonic Detection of Fiber Orientation in Composite Laminates for Use of Vehicular Structures,” *Key Engineering Materials*, Vol. 297–300, Pages. 2109–2114, 2005, doi: 10.4028/www.scientific.net/KEM.297-300.2109.
[10] S. Tsai and E. Wu. A General Theory of Strength for Anisotropic Materials. *Technical Report AFML*-TR-71-12, August 1972.
[11] R. M. Narayanan, “Microwave Nondestructive Testing of Galvanic Corrosion and Impact Damage in Carbon Fiber Reinforced Polymer Composites,” *International Journal of Microwaves Applications*, Vol. 7, Issue. 1, Pages. 1–15, Feb. 2018, doi: 10.30534/ijma/2018/01712018.
[12] B. Yang, Y. Chen, J. Lee, K. Fu, and Y. Li, “In-plane compression response of woven CFRP composite after low-velocity impact: Modelling and experiment,” *Thin-Walled Structures*, Vol. 158, Jan. 2021, doi: 10.1016/j.tws.2020.107186.
[13] H. M. Gomes, “Reliability based optimization of laminated composite structures using genetic algorithms and Artificial Neural Networks,” *Structural Safety*, Jan. 2011, [Online]. Available: https://www.academia.edu/32950193/Reliability_based_optimization_of_laminated_composite_structures_using_genetic_algorithms_and_Artificial_Neural_Networks
[14] C. M. Bishop, “Pattern Recognition and Machine Learning,” *Springer*, 2006.